# Arsenic disrupts extracellular vesicle-mediated signaling in regenerating myofibers

Zachary Clemens ![ORCID],[1] Kai Wang,[2,3] Fabrisia Ambrosio,[2,3,*] Aaron Barchowsky ![ORCID][1,*]

[1]Department of Environmental and Occupational Health, University of Pittsburgh School of Public Health, Pittsburgh, Pennsylvania, USA
[2]Discovery Center for Musculoskeletal Recovery, Schoen Adams Research Institute at Spaulding, Boston, Massachusetts, USA
[3]Department of Physical Medicine and Rehabilitation, Harvard Medical School, Boston, Massachusetts, USA

*To whom correspondence should be addressed at Public Health Building 4133, 130 De Soto Street, Pittsburgh, PA 15261, USA. E-mail: aab20@pitt.edu and Office 5304, 149 13th Street, Charlestown, MA 02129, USA. E-mail: fambrosio@mgh.harvard.edu.

Zachary Clemens and Kai Wang contributed equally to this study.

## Abstract

Chronic exposure to environmental arsenic is a public health crisis affecting hundreds of millions of individuals worldwide. Though arsenic is known to contribute to many pathologies and diseases, including cancers, cardiovascular and pulmonary diseases, and neurological impairment, the mechanisms for arsenic-promoted disease remain unresolved. This is especially true for arsenic impacts on skeletal muscle function and metabolism, despite the crucial role that skeletal muscle health plays in maintaining cardiovascular health, systemic homeostasis, and cognition. A barrier to researching this area is the challenge of interrogating muscle cell-specific effects in biologically relevant models. *Ex vivo* studies investigating mechanisms for muscle-specific responses to arsenic or other environmental contaminants primarily utilize traditional 2-dimensional culture models that cannot elucidate effects on muscle physiology or function. Therefore, we developed a contractile 3-dimensional muscle construct model—composed of primary mouse muscle progenitor cells differentiated in a hydrogel matrix—to study arsenic exposure impacts on skeletal muscle regeneration. Muscle constructs exposed to low-dose (50 nM) arsenic exhibited reduced strength and myofiber diameter following recovery from muscle injury. These effects were attributable to dysfunctional paracrine signaling mediated by extracellular vesicles (EVs) released from muscle cells. Specifically, we found that EVs collected from arsenic-exposed muscle constructs recapitulated the inhibitory effects of direct arsenic exposure on myofiber regeneration. In addition, muscle constructs treated with EVs isolated from muscles of arsenic-exposed mice displayed significantly decreased strength. Our findings highlight a novel model for muscle toxicity research and uncover a mechanism of arsenic-induced muscle dysfunction by the disruption of EV-mediated intercellular communication.

**Keywords:** arsenic; extracellular vesicles; skeletal muscle; bioengineered tissue; regeneration

By mass alone, skeletal muscles account for nearly half of human bodyweight and skeletal muscles play a crucial role in metabolism, homeostasis, and endocrine signaling (Egan and Zierath, 2013; Frontera and Ochala, 2015; Giudice and Taylor, 2017). The ability to perform these roles strongly predicts fitness, health (physical and mental), and even mortality (Janssen *et al.*, 2020; Marques *et al.*, 2020; Metter *et al.*, 2002; Samuel *et al.*, 2012). Despite its importance, muscle health receives relatively little attention in the field of environmental toxicology.

The gap in our understanding of muscle contribution to the pathogenic progression of disease is especially notable in the case of arsenic exposure. Worldwide, over 200 million people consume water with arsenic levels exceeding the WHO standard for safety of 10 ppb (Gorchev and Ozolins, 1984; Podgorski and Berg, 2020). The cardiometabolic disease burden associated with arsenic exposure is estimated at nearly 50 million disability-adjusted life years annually (Oberoi *et al.*, 2019). Additionally, more than 10 million people worldwide suffer from skeletal muscle dysfunction related to arsenic exposure (Mondal *et al.*, 2020; Mukherjee *et al.*, 2003; Parvez *et al.*, 2011; Sarker *et al.*, 2021).

Skeletal muscle health and cardiometabolic disease are inextricably linked. Insulin resistance in skeletal muscle is a hallmark of diabetes onset (DeFronzo and Tripathy, 2009; Goodpaster *et al.*, 2003), and resistance muscle training increases the ability to regulate blood sugar in people with diabetes (Lee *et al.*, 2017). Arsenic exposures that impair muscle health have been associated with increased hyperglycemia and insulin resistance (Mondal *et al.*, 2020). Muscle health is also a strong predictor of morbidity and mortality in patients with heart failure or after cardiovascular surgery (Kumar *et al.*, 2019; von Haehling *et al.*, 2020; Yamashita *et al.*, 2021). Despite their clear connection, many studies focus on arsenic-associated cardiovascular risk (Alamolhodaei *et al.*, 2015; Balakumar and Kaur, 2009), whereas few consider muscle-specific effects of arsenic exposure.

An important dimension to consider in studying arsenic effects on muscle cells is the contribution of intercellular and paracrine communication. The importance of muscle to systemic communication is demonstrated by experiments that show improved muscle regeneration in old mice when their circulatory systems were joined with those of young mice (Conboy *et al.*, 2013).

This was attributed to circulating factors that can enhance muscle stem cell (MuSC) activation and myogenic differentiation (Conboy et al., 2005). Recent work identified extracellular vesicle (EV) communication as a major contributor to muscle-generated paracrine and systemic signaling (Choi et al., 2016; Sahu et al., 2021). EVs are membrane-encapsulated nanoparticles that carry lipid, protein, and nucleic acid cargo (Van Niel et al., 2018). MuSCs and muscle fibers release EVs that contribute to the activation and differentiation of recipient MuSCs (Choi et al., 2016), suggesting that cell-autonomous paracrine signaling helps drive the regenerative cascade in muscle. Although arsenic is known to influence EV cargoes of cancer stem cells and to disrupt embryonic EV signaling for proper stem cell differentiation (Bain et al., 2016; Li et al., 2021; Ngalame et al., 2018; Wang et al., 2021), little is known of the effects of arsenic on generation of pathogenic EV cargo from noncancer tissues, such as skeletal muscle, that can impair tissue maintenance and regeneration.

Studying the skeletal muscle-specific effects of arsenic poses a significant challenge. In addition to myofibers and muscle progenitors, numerous other cell and tissue types make up the muscle milieu, and many of these cell populations respond to arsenic (Giles and Mann, 2022; States et al., 2009; Zhang et al., 2016a), making it difficult to extract cell- or tissue-specific effects. Previous in vitro studies suggested that arsenic targets MuSCs and progenitor cells directly by disrupting bioenergetics, inducing aberrant mitochondrial function, and altering the extracellular matrix environment (Ambrosio et al., 2014; Anguiano et al., 2020; Cheikhi et al., 2020). Accordingly, exposing mice to arsenic in their drinking water for 4–5 weeks resulted in impaired muscle regeneration, increased fatigue susceptibility, and increased intramuscular lipid accumulation (Ambrosio et al., 2014; Chen et al., 2020; Garciafigueroa et al., 2013; Zhang et al., 2016a). However, both in vitro and in vivo studies of arsenic and muscle cells have limitations. The main limitation of 2D in vitro muscle cell models is that they are static and do not provide a physiologically relevant environment for the muscle cells. In contrast, the major limitation of in vivo models is the difficulty in identifying muscle-specific effects of arsenic exposure in the context of the additional components present in muscle. Thus, new models are necessary for studying the pathogenic muscle-specific effects of arsenic.

The development of 3D cell culture models offers great promise for using a reductionist approach to address the above-mentioned challenges and gaps. Recently, models have been developed to study skeletal muscle growth and function (Dessauge et al., 2021; Fleming et al., 2020). Muscle constructs generated from purified muscle progenitor cells (MPCs) recapitulate in vivo function without the confounding presence of nonmuscle components in the intact muscle. These characteristics offer great potential for environmental toxicology in muscle. We sought to harness the advantages offered by 3D systems to study arsenic effects on skeletal muscle and to explore the importance of EV-mediated communication in the pathogenic response to arsenic exposure. To test this hypothesis, we developed and employed functional 3D muscle constructs using primary mouse MPCs. We used these models to demonstrate that arsenic impairs regeneration through elaboration of a dysfunctional cellular secretome, mediated by EVs. This heretofore unknown mechanism of arsenic-induced muscle damage offers a promising avenue for further investigation and, potentially, therapeutic interventions.

## Materials and Methods

### Scientific rigor and reproducibility

In vitro experiments involving muscle constructs were conducted with a minimum of 5 technical replicates per group. Constructs with visible structural deficits were excluded prior to experiments. Other in vitro culture experiments were repeated at least twice with 3–4 wells used per group. All in vitro experiments were repeated to ensure reproducibility. In vivo experiments were conducted with a group size of 8 animals split between 2 cohorts and performed across multiple days. Comparisons were made between cohorts to ensure the absence of a cohort effect. Group sizes were estimated using an online power analysis tool (clincalc.com). Researchers remained blinded to treatments throughout experiments. Antibody information is provided as Table 1 and the source for other important materials are referenced.

### Animal experiments and ethics

All animal experiments were approved by the Institutional Animal Care and Use Committee (IACUC) at the University of Pittsburgh. The C57 BL/6J male mice used for these experiments were obtained from Jackson Laboratories. All animals were acclimatized for at least 72 h after delivery prior to use in any experiments. Experiments were conducted in accordance with protocol 22112013 (University of Pittsburgh ARO: IS00022013).

### Preparation of muscle constructs

Primary MPCs isolation and muscle construct preparation were performed based on our previously published protocol (Sahu et al., 2018). Briefly, mouse skeletal muscles from 3 to 5 month old male mice were enzymatically digested by collagenase II and dispase. MPCs were then enriched using a preplating technique (Wang et al., 2023). Polydimethylsiloxane (PDMS) muscle construct frames (Supplementary Data A—Figure 1) were assembled based on our previous work (Wang et al., 2023) and sterilized with 70% ethanol and UV treatment for 30 min each. To prepare muscle constructs, $2 \times 10^6$ cells were suspended in 71.2 µl proliferation medium followed by adding 0.8 µl Thrombin (Millipore

**Table 1.** Immunofluorescence Information

| Antibody/Target | Source/Catalog No. | Dilution | Complementary Secondary Antibody (Source) | Secondary Dilution |
|---|---|---|---|---|
| Sarcomeric alpha-actinin | Invitrogen MA1-22863 | 1:200 | Goat anti-mouse IgG1 594 (Invitrogen A21125) | 1:500 |
| Embryonic myosin heavy chain (eMHC) | DSHB F1.652 | 1:150 | Goat anti-mouse IgG1 594 (Invitrogen A21125) | 1:500 |
| Desmin | Abcam ab15200 | 1:500 | Goat anti-rabbit 488 (Invitrogen A11034) | 1:500 |
| CD63 (AlexaFluor 488 conjugated) | Santa Cruz sc-5275 AF488 | 1:500 | N/A | N/A |
| DAPI | Center for Biologic Imaging (CBI) University of Pittsburgh | 1:5 | N/A | N/A |

Sigma, 100 U/ml in PBS containing 0.1% bovine serum albumin [BSA]), 20 µl Matrigel (Corning), and 8 µl Fibrinogen (Millipore Sigma, 50 mg/ml in PBS). Eighty-five microliters of the mixture of cells and hydrogels was then added to the sterilized muscle construct frame and incubated for 20 min at 37°C for gelation. Muscle constructs were cultured in proliferation medium (without bFGF) containing 1.5 mg/ml 6-aminocaproic acid (ACA; Sigma-Aldrich) for 4 days, followed by culturing in differentiation medium supplemented with 2 mg/ml ACA for another 14 days to induce MPC differentiation. The muscle construct frame contains 2 anchors on each side to induce the alignment of formed myotubes.1

### Construct arsenic exposure and injury

After 14 days of differentiation, muscle constructs were cultured in differentiation media containing 0–100 nM arsenic (in the form of NaAsO$_2$) for another 10 days. The constructs were rinsed with arsenic-free medium and were then injured through incubation with differentiation media containing 0.4 µM cardiotoxin (Sigma-Aldrich 217503) for 5 h based on our previously developed protocol (Wang et al., 2023). After injury, muscle constructs were cultured in arsenic-free differentiation media to allow myotube regeneration. Contractile force testing (described next) was then conducted 7 days post injury (DPI).

### Measurement of construct contractile forces

The contractile force measurement was conducted as previously described (Wang et al., 2023). Briefly, muscle constructs were attached to hooks that were connected to a force transducer (Model 405A, Aurora Scientific, Inc., Ontario, Canada) and length controller (Model 322C, Aurora Scientific, Inc.). The constructs were then immersed in oxygenated Tyrode's solution (5 mM HEPES, 5 mM glucose, 2.5 mM CaCl$_2$, 2.1 mM MgCl$_2$, 5.5 mM KCl, 134 mM NaCl, and 0.33 mM NaH$_2$PO$_4$, pH 7.4), warmed at 37°C, and stretched to 110% of their original length. The twitch and tetanic contractile forces were recorded in response to 10 ms electrical pulses applied by platinum electrodes at 1 Hz and 40 Hz stimulation rates, respectively. For fatigue resistance tests, muscle constructs were continuously stimulated for 30 s under 40 Hz. The force values after stimulation were normalized to the tetanic force value right begin electrical stimulation to obtain the percentage of force drop. Higher levels of force drop indicated less resistance to fatigue. Force data were collected using ASI600 software (Aurora Scientific, Inc.) and analyzed in Microsoft Excel. Due to a change in lab location, a new instrument was used to collect data presented in Figure 5.

### Muscle construct-conditioned media treatment

Constructs were exposed to 50 nM arsenic and injured as described earlier. Two-days after the injury, we collected the conditioned media from the constructs (approximately 1.5 ml per construct). Media from each construct were concentrated to a volume of 50–70 µl using 10 kDa molecular-weight cutoff centrifugal filter units (Amicon UFC901024). Mature constructs were injured and treated directly with un-concentrated conditioned media, or with fresh media supplemented with concentrates of control or arsenic-exposed construct conditioned-media at 2, 4, and 6 DPI prior to construct contractile testing and fixation.

### Extracellular vesicle isolation and characterization

EVs were isolated using size-exclusion chromatography (SEC) columns (iZon ICO-35). Culture media was concentrated to a volume of approximately 500 µl using 100 kDa centrifugal filter units (Amicon UFC910024). This concentrated media was then run through the SEC columns and the 1.9–3.5 ml fraction was collected. Nanoparticle tracking analysis (NTA) using a NanoSight NS-300 (Malvern Panalytical) was used to characterize EV concentration and size. Samples were diluted 1:100 and 3 60-s videos were captured for each sample.

ImageStream flow cytometry was used to validate EV tetraspanin expression. Briefly, 140 µl of each EV sample was fixed with an equal volume of 4% PFA for 10 min, then spun at 30 000 × g and supernatant discarded. Blocking was achieved using 3% BSA for 1 h, followed by another spin. A primary antibody for CD63 (Table 1) was added and incubated overnight. Stained samples were analyzed at 60× using an ImageStream flow analyzer (Amnis Mark II). Analysis was conducted using the IDEAs software.

### Muscle-EV collection

Male C57 BL/6J (Jackson Laboratories) mice were given spring water or spring water containing 100 ppb arsenic (in the form of sodium arsenite) in their drinking water beginning at 6-weeks old and lasting for 5 weeks. After 5 weeks, the arsenic was removed and the tibialis anterior (TA) muscles were injured via a bilateral intramuscular injection of 10 µl cardiotoxin (Clemens et al., 2021). Subcutaneous injection of Rimadyl provided pain relief. At 14 DPI, animals were euthanized, and TA muscles were excised. The TAs were then finely minced in a petri dish containing DMEM, rinsed with DMEM, and plated for 24 h to condition medium with EVs. The conditioned media was then centrifuged at 2000 × g for 20 min to remove cells, fibers, and debris. The supernatant was then centrifuged at 10 000 × g for 30 min, and the resultant supernatant was passed through a 0.22 µm filter (Aswad et al., 2014). The filtered solutions were cleared of smaller proteins and molecules, as well as concentrated to <500 µl using 100 kDa cut-off centrifugal filter columns. EVs were isolated from the concentrates by SEC as dcribed earlier.

### Muscle construct EV treatment

Serum-free differentiation media was prepared using DMEM and 2% N$_2$ supplement. Mature constructs were injured and treated at 2, 4, and 6 DPI with serum-free differentiation media containing EVs from unexposed or arsenic-exposed mouse TA muscles. The dose used was 3 × 10$^8$ EVs/construct/treatment.

### *In vivo* EV injections and contractile testing

Six-week-old male mice were exposed to arsenic water (100 ppb) or control water for 5 weeks as described earlier. The TAs were then injured by injecting 20 µl 1.2% barium chloride into each muscle (Anguiano et al., 2020). Barium chloride and cardiotoxin injuries are highly similar in the extent of tissue damage and in the recovery process, but barium chloride is less prone to batch variations in potency and was thus chosen for the *in vivo* contractile testing experiments (Hardy et al., 2016). At 24 and 72 h after the injury, EVs were injected into the TA using a 31G needle at a dosage of 7.5 × 10$^8$ EVs/injection. The injection volume was 30 µl. Pain relief was provided via subcutaneous injection as above. At 14 DPI, animals underwent *in vivo* contractile testing based on a previously established method (Clemens et al., 2021). The surgically exposed peroneal nerve was stimulated by an electrode, inducing TA dorsiflexion which was measured by a force transducer footplate. Three contractile paradigms were used. (1) Single-twitch protocol in which 6 single-pulse stimulations were delivered at 5-s intervals. (2) Force-frequency protocol in which 9 tetanic stimulations (350 ms stimulation) of increasing frequency

(10, 30, 50, 80, 100, 120, 150, 180, and 200 Hz) were delivered at 2-min intervals. (3) Fatigue-recovery protocol in which 104 tetanic stimulations (100 Hz, 350 ms) were delivered at an interval of 4-s to induce muscle fatigue. Recovery was assessed by stimulation (100 Hz, 350 ms) at 5 and 10 min following the end of the fatigue cycle.

## Muscle construct immunostaining and imaging

All incubation steps took place using microcentrifuge tubes in a tube rotator. Muscle constructs were removed from their PDMS molds and fixed in 2% PFA overnight, then washed in PBS 3 times for 10 min each. Fixed constructs were blocked in PBS with 0.2% Triton-X, 10% normal goat serum (NGS), and 3% BSA for 3 h at room temperature. Next, primary antibodies (Table 1) were diluted in PBS with 5% NGS, and constructs were incubated with the primary antibodies overnight at 4°C. After washing 3 times for 5 min, secondary antibodies (Table 1) diluted in PBS with 5% NGS were added for 3 h at room temperature. Constructs were then washed 3 times with PBS, then incubated with 4′,6-diami-dino-2-phenylindole (DAPI, 1:500 dilution) for 3 min and washed twice more.

The muscle constructs were imaged on a Nikon A1 confocal microscope at 60× magnification. The constructs were placed on a microscope slide coverslip on the stage with a drop of PBS added to prevent them from drying out during imaging. Approximately 10 μm thick Z-stack images were collected with slice thickness of 0.4–0.6 μm. Maximum intensity projections were then created from these Z-stacks for analysis. Fiber diameter analysis was conducted using NIS-Elements. Three diameters were measured at different points along each fiber and averaged. Alpha-actinin staining was used to count striated fibers.

## Proteomics acquisition and analysis

The arsenic treatment and muscle construct injury were conducted as described earlier. After injury, muscle constructs were cultured in a DMEM media containing N2 supplement (Gibco) for 2 days. Conditioned media (1.5 ml) was then collected and concentrated to less than 50 μl using 10 kDa cutoff centrifugal filter units (UFC901024). Mass spectrometry analysis was performed by Tymora Analytical Operations (West Lafayette, Indiana). KEGG and GO enrichment analyses of the proteins that showed significant differences between arsenic and control muscle construct conditioned media were performed by shiny GO online tools (version 0.76.3).

## C2C12 culture and EV treatment

C2C12 cells proliferated in DMEM (Gibco 12430-054) containing 10% FBS (Cytiva SH30071.03) and 1% pen/strep (Gibco 15-140-122). Once cells reached approximately 80% confluency they were differentiated in low-serum media composed of DMEM, 2% horse serum (Cytiva SH30074.03), and 1% pen/strep. For arsenic preexposure, cells were exposed to 50 nM arsenic during differentiation for 4 days. Next, cells were trypsinized and passed through a 40-μm filter to collect the undifferentiated "reserve" cells (Cheikhi et al., 2019). These cells were then plated and proliferated again until 80% confluency was reached. Then, they were differentiated and treated with equal quantities of arsenic-EVs, control-EVs, or no EVs in medium with horse serum depleted of EVs by ultracentrifugation. EV treatment occurred every 2 days starting at the time of differentiation. The dose used was $5 \times 10^7$ EVs/cm$^2$.

## Immunocytochemistry, imaging, and analysis

C2C12 cells grown in 24-well plates were fixed in 2% PFA for 10 min, then washed 3 times with 1× PBS for 2 min each. If staining was not to be performed immediately, fixed plates were stored with PBS at 4°C. Fixed cells were permeabilized with 0.1% Triton-X in PBS for 15 min at room temperature. Next, blocking was performed using 0.1% Triton-X + 3% BSA in PBS for 1 h at room temperature. Primary antibodies (Table 1) were diluted in 0.1% Triton-X + 3% BSA + 5% NDS then added to the cells to incubate overnight at 4°C. After 3 2-min PBS washes, cells were incubated with secondary antibodies (Table 1), using the same diluent as the primary antibodies for 1 h at room temperature in the dark. Lastly, cells were washed 3 times in PBS, incubated with DAPI for 1 min, then washed 2 more times.

Imaging was conducted at 20× magnification using a Keyence BZ-X810 (Keyence Corporation of America). A 5 × 5 field of images was stitched together for each well. All analysis was performed using ImageJ. Area coverage was quantified by thresholding for positive signal, then measuring percent area. For myotube width, a 7 × 5 grid of was overlaid on the image. Myotube width was measured manually for the single fiber nearest to each of the interior intersection points for a total of 24 fibers per image.

## Transmission electron microscopy

Muscle constructs were fixed in 2.5% glutaraldehyde in 1× PBS overnight then washed 3 times with PBS for 15 min each. They were then postfixed in aqueous 1% osmium tetroxide overnight, and washed 3 more times. Next, they were dehydrated through a 30%–100% ethanol series (15 min each) and 2 changes of propylene oxide (15 min each). Constructs were then infiltrated with a 1:1 mix of propylene oxide and epon overnight. Next, they were infiltrated with pure epon and embedded in epon for 24 h at 37°C before curing for 48 h at 60°C. Ultrathin cross sections (60 nm) of the cells were obtained on a Reichert Ultracut E microtome, post-stained in 4% uranyl acetate for 10 min and in 1% lead citrate for 7 min. Sections were imaged at 50 000× magnification using a JEOL 1400-PLUS 120 kV TEM at 80 kV. Images were taken using a side-mount AMT 2k digital camera (Advanced Microscopy Techniques).

## Statistical analysis

Statistical tests were performed using GraphPad Prism (9.5.0) or Microsoft Excel. Prior to hypothesis testing, a Shapiro-Wilk test was conducted to assess the normality of the data. Data with normal distributions were compared using student's t-tests or 1-way ANOVA with Tukey's multiple comparisons post-hoc test. Data with nonnormal distributions were compared using a Mann-Whitney rank comparison test or Kruskal-Willis test with Dunn's multiple comparison. A p-value less than .05 was considered statistically significant. All data are displayed as mean ± standard error of the mean (SEM). A nonlinear least squares regression model was used to generate 1-phase decay equations modeling fatigability. The parameters were compared using multiple extra-sum-of-squares F tests.

# Results

## Development of a model to isolate cell-specific arsenic exposure effects

We adapted the cultured 3D muscle construct model of Wang et al. (2023) to elucidate the muscle cell- and fiber-autonomous effects of arsenic exposure. Skeletal MPCs (MPCs) were isolated from 3- to 5-month-old male C57BL/6J mice using a modified pre-plating technique which yields an approximately 92% pure population of MPCs (Sahu et al., 2018; Wang et al., 2023). After
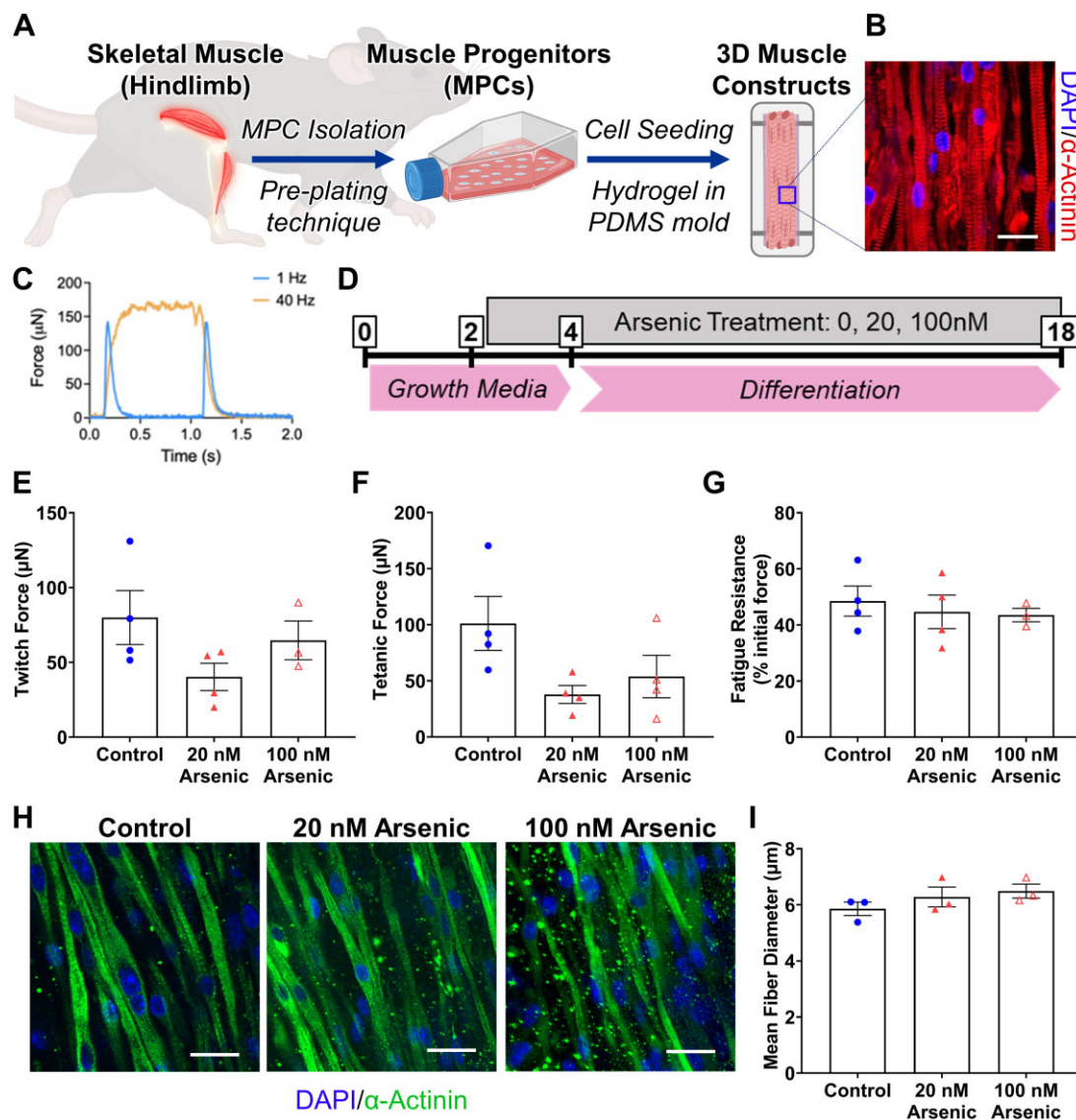
**Figure 1.** 3D muscle constructs model environmental arsenic exposure. A, Schematic outlining the process for fabricating 3D muscle constructs from mouse MPCs. B, Representative image of muscle construct stained for nuclei (blue) and α-actinin (red, scale bar = 20 μm). C, Representative graph showing contractile force of muscle constructs. Single-twitch stimulation peaks are shown in blue, with tetanic stimulation curve at 40 Hz shown in orange. D, Experimental scheme for construct exposure to arsenic at various concentrations (time scale indicates days). E, Single-twitch force in unexposed and arsenic-exposed constructs measured by contractile testing ($N = 11$, 1-way ANOVA). F, Maximum tetanic force ($N = 12$, 1-way ANOVA). G, Percentage of muscle construct force drop after 30-s stimulation at 40 Hz ($N = 12$, Kruskal-Wallis test). H, Representative images of constructs stained for DAPI (blue) and α-actinin (green, magnification = 40×, scale bars = 20 μm). I, Mean fiber width quantified from immunofluorescence staining of muscle constructs ($N = 9$, Kruskal-Wallis test).

expansion, MPCs were mixed with hydrogels composed of Matrigel and fibrinogen and seeded into a PDMS mold (Figure 1A). After 2 weeks of myogenic differentiation, the constructs formed aligned fibers with visible striations (Figure 1B) and displayed quantifiable contraction when electrically stimulated (Figure 1C). As an initial investigation of the effects of arsenic exposure on myogenesis, constructs were treated with 0, 20, or 100 nM of arsenite, beginning 2 days after cell seeding and through the 2 weeks of differentiation (Figure 1D). The concentration range is relevant to expected human tissue concentrations, because humans drinking water containing 100 ppb arsenic have average blood levels of 90 nM (Hall et al., 2006; Parvez et al., 2011), and arsenic-impaired motor function is observed in children with average blood levels of 43 nM (Parvez et al., 2011). Although there were trends toward a loss of contractile strength with exposure,

differences between groups were not significant (Figs. 1E and 1F). Fatigue resistance of the muscle constructs, assessed by continuously stimulating muscle constructs and quantifying the percentage of force drop, also trended towards inhibition by arsenite (Figure 1G). Morphologically, as assessed via immunofluorescence staining for sarcomeric α-actinin, fibers developed in the presence of arsenic appeared misshapen with more globular structure (Figure 1H) and trend toward a hypertrophic phenotype with increased diameter (Figure 1I). These results are consistent with previous in vivo observations demonstrating that, in the absence of an additional stressor, such as a muscle injury, arsenic exposure alone does not overtly compromise muscle strength and may induce muscle hypertrophy (Ambrosio et al., 2014).

As with arsenic-promoted carcinogenesis, arsenic acts as an enhancer with its pathogenic effects often not revealed without

additional insults or genetic changes (States *et al.*, 2011). Arsenic exposure followed by muscle injury consistently reduces muscle recovery in arsenic-exposed mice, producing reduced force and fatigue recovery capacity (Ambrosio *et al.*, 2014; Anguiano *et al.*, 2020; Zhang *et al.*, 2016a). Therefore, we next adapted a model of *in vivo* muscle injury to use with our 3D constructs. We exposed mature constructs to 50 nM arsenic for 10 days, removed the arsenic, and then incubated constructs with 0.4 μM cardiotoxin for 5 h to induce muscle injury (Figure 2A). Cardiotoxin induces fiber necrosis and fragmentation with reduced contractility, which will repair over 2 weeks *in vivo* (Wang *et al.*, 2023). This exposure and injury model is consistent with our *in vivo* injury models of providing young adult mice arsenic in their drinking

water for 5 weeks, removing the arsenic, injuring with either cardiotoxin or barium chloride, and allowing 2 weeks of recovery in the absence of arsenic before contractile testing and tissue analysis (Anguiano *et al.*, 2020; Zhang *et al.*, 2016a). We previously found that arsenic exposure does not increase susceptibility to or the extent of cardiotoxin injury *in vivo*, but instead impairs the recovery program (Zhang *et al.*, 2016a). Thus, we allowed injured constructs to recover in arsenic-free differentiation media for 7 days, then tested the physiological function of fibers. Recovery of twitch and tetanic force following injury was 25% less in the arsenic-exposed constructs, relative to control constructs (Figure 2B). In contrast to effects on fiber development (Figs. 1H and 1I), at both 2 and 7 DPI, regenerated fiber diameter was
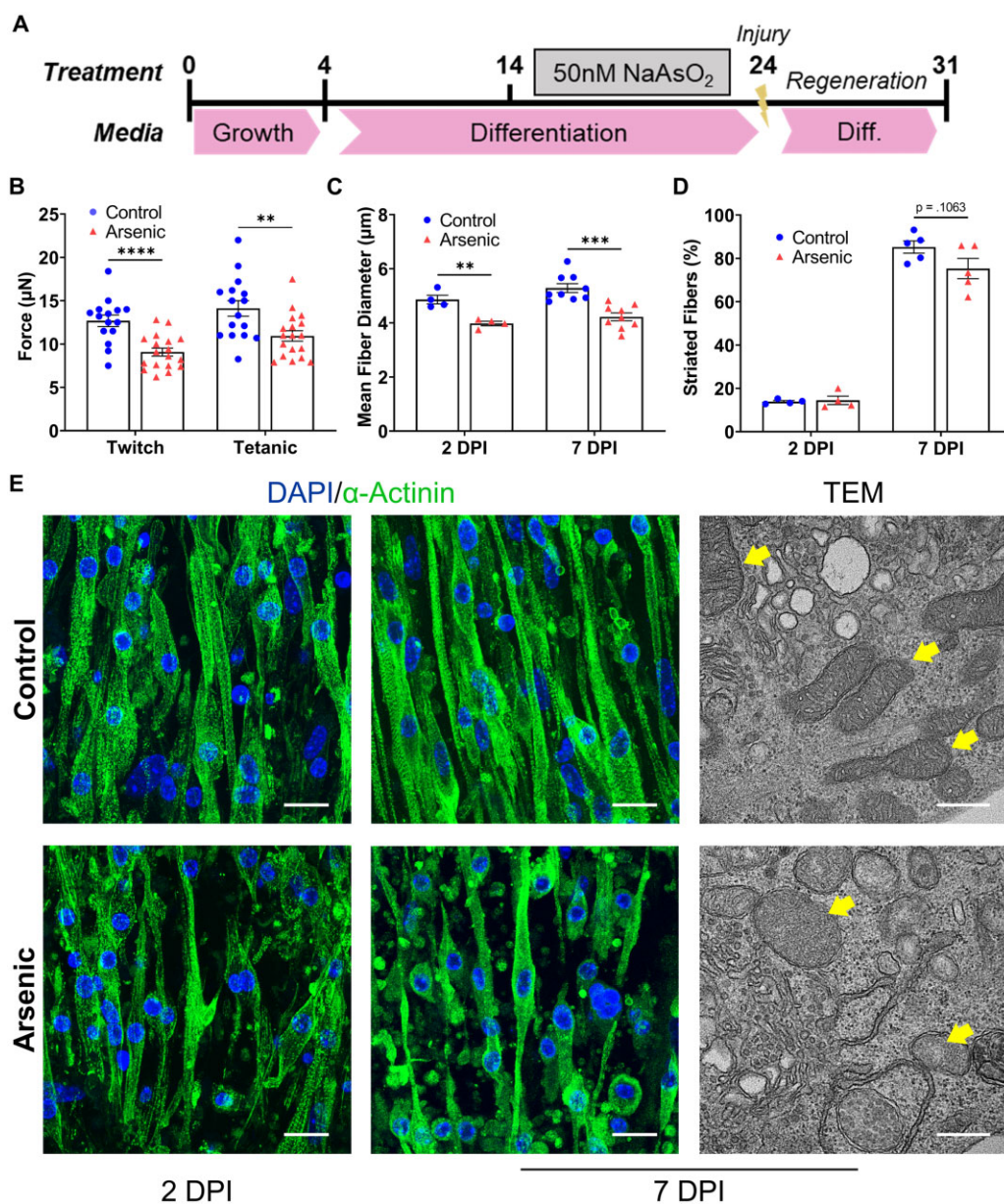


**Figure 2.** Arsenic-exposed muscle constructs display impaired regeneration. A, Experimental design for arsenic exposure and injury in muscle constructs (time scale indicates days). B, Single-twitch ($N = 33$) and tetanic ($N = 34$) contractile force in muscle constructs 7 DPI (Student's *t*-tests, ** $p <$ .01, **** $p <$ .0001). C, Mean fiber width of muscle constructs at 2 DPI ($N = 8$) and 7 DPI ($N = 18$, Student's *t*-tests, ** $p <$ .01, *** $p <$ .001). D, Percent of fibers with visible striations at 2 DPI ($N = 8$) and 7 DPI ($N = 10$, Student's *t*-tests). E, Representative images of (left columns) constructs stained for DAPI (blue) and alpha-actinin (green, magnification = 60×, scale bars = 20 μm) at 2 and 7 DPI, and (right column) MuSCs in constructs imaged via TEM at 7 DPI (magnification = 50 000×, scale bars = 400 nm). Arrows in TEM images indicate qualitative differences in mitochondrial integrity between conditions.

approximately 20% lower in the arsenic-exposed constructs (Figs. 2C and 2E). Striations indicate the formation of organized contractile sarcomeres in the regenerated fibers. Arsenic exposed constructs trended toward a reduced proportion of structures with defined striations at 7 DPI, relative to the more developed fibers in the controls (Figs. 2D and 2E). Note that 2 DPI in the regeneration process is a proliferative phase where there are few regenerated fibers in either control or arsenic-exposed constructs relative to 7 DPI (Figure 2D). As in Figure 1I, structures in 7 DPI arsenic-exposed constructs appeared to be more globular with fewer multinucleated fused structures, relative to control (Figure 2E).

We previously demonstrated that muscle and MPC mitochondria are a primary target for arsenic-impaired myogenic differentiation and muscle regeneration, exhibiting abnormal morphology, dysregulated membrane potential, and increased reactive oxygen species generation, all contributing to reduced cell differentiation (Ambrosio et al., 2014; Anguiano et al., 2020; Cheikhi et al., 2019; al., 2020). Consistent with observations of loss of mitochondrial integrity in arsenic-exposed muscle in vivo (Ambrosio et al., 2014; Bae et al., 2019; Prakash et al., 2022), TEM imaging revealed that mitochondria of arsenic-exposed constructs had qualitative disruption of the cristae, as well loss of mitochondrial membrane integrity (Figure 2E). Taken together, these studies showed that the cultured 3D muscle constructs replicated arsenic-induced dysfunctional muscle regeneration in vivo (Ambrosio et al., 2014; Zhang et al., 2016a), attesting to their validity as a model to explore the mechanisms responsible for these findings. Absence of arsenic during the recovery phase suggested a preinjury effect on the capacity to regenerate, rather than direct inhibition during the regeneration process.

### Secreted factors contribute to arsenic-induced impairment of muscle regeneration

The reduced regenerative capacity could result from disrupting the intercellular and paracrine communication crucial for healthy muscle regeneration (Demonbreun and McNally, 2017; Mitchell et al., 2019; Sahu et al., 2021). Given that arsenic stimulates the release of extracellular factors that can impact function in cells not directly exposed to arsenic (Anguiano et al., 2020), we evaluated the relative contribution of arsenic-disrupted paracrine signaling during skeletal muscle regeneration. We used the same exposure protocol as seen in Figure 2A to expose mature constructs to 50 nM arsenic followed by an injury. After the injury, the constructs were rinsed and fresh arsenic-free differentiation media was added. Conditioned media was collected from regenerating constructs at 2 DPI and used to treat nonarsenic exposed, injured constructs during regeneration (Figure 3A). Unexpectedly, we found that force production of constructs treated with conditioned media from arsenic constructs was significantly greater than injured constructs treated with media from control counterparts, though fiber diameter was unaffected (Supplementary Data A—Figure 2). We hypothesized that this paradoxical finding may have resulted from control media becoming more depleted of nutrients due to more robust metabolism in the control constructs. To test this possibility, we repeated the experiment, but concentrated the conditioned media from the control or arsenic-exposed constructs using centrifugal filtration. We then diluted the control or arsenic-conditioned concentrates 40-fold in replete recovery medium and cultured the naïve, injured constructs for 7 DPI. Following this latter paradigm, the initial results were reversed and recovery of contractile force was roughly 50% lower

in naïve constructs incubated with arsenic-conditioned media concentrate compared with control-conditioned media concentrate (Figure 3B). As above, there was a trend towards smaller fiber diameter and fewer striated fibers in the group recovering in arsenic-conditioned media relative to control-conditioned media (Figs. 3C–E).

The findings suggested that arsenic exposure inhibits the release of paracrine factors required for regeneration or promotes a pathogenic secretome that inhibits the regenerative process even in the absence of arsenic. Thus, we next investigated potential molecular drivers of the adverse effect of the arsenic-conditioned secretome on functional regeneration. To this end, we used mass spectral analysis to compare the proteomes in the concentrated control or arsenic-conditioned media samples ($n = 4$/group). In total, we identified 222 differentially abundant proteins, with 118 increasing in abundance following arsenic-exposure and 104 decreasing in abundance (Figs. 3F and 3G). KEGG pathways and GO terms were associated with the differentially abundant proteins (Figs. 3H and 3I). The top pathways identified were complement and coagulation cascades, PI3K-Akt signaling, and regulation of actin cytoskeleton—known contributors to muscle development and regeneration (Clarkson et al., 2004; Elia et al., 2007; Wang et al., 2023). Additionally, ECM-receptor interactions were near the top of the list, consistent with known effects of arsenic exposure on connective tissue fibroblasts (Anguiano et al., 2020; Zhang et al., 2016a). A complete list of the proteins identified in our dataset is available as Supplementary Data B.

### Extracellular vesicles are vehicles of arsenic-induced dysfunctional communication

The proteins identified from our mass spectrometry dataset could either be unbound or packaged within EVs. EV-mediated communication plays a crucial role in muscle regeneration through lipid, nucleic acid, and protein trafficking and uptake in distant cells and tissues (Mitchell et al., 2019; Sahu et al., 2021). Therefore, we investigated the contribution of dysfunctional EV signaling to arsenic-impaired regeneration. We collected conditioned media from control and arsenic-exposed constructs following the injury-recovery protocol above and isolated EVs via SEC (Figure 4A). The size and number of EVs isolated from concentrated control conditioned media (Ct-EVs) and concentrated arsenic-conditioned media (As-EVs) were characterized via NTA (Supplementary Data A—Figs. 3A and 3B). As-EVs were slightly larger in mean diameter than Ct-EVs (88 nm vs 78 nm) but median diameter and EV concentration were not different (Supplementary Data A—Figure 3B). We also confirmed the enrichment of tetraspanin EV proteins using Imagestream flow cytometric analysis (Supplementary Data A—Figs. 3C and 3D).

We next tested the effects of these isolated EVs on muscle progenitor differentiation. We differentiated C2C12 myoblasts with low-serum (2% EV-free horse serum) media supplemented with either Ct-EVs or As-EVs for 5 days (Figure 4A). We also included a group receiving the same differentiation media without EV supplementation (no EVs) as a separate control, because serum EVs significantly contribute to proper myogenic differentiation (Aswad et al., 2016). Cultures receiving As-EVs or no EVs showed approximately 10% less desmin coverage (area of the well covered by desmin positive structures) and nearly 30% fewer embryonic myosin heavy chain (eMHC) positive multinucleated structures, 2 markers of early muscle fiber differentiation, when compared with cells treated with Ct-EVs (Figs. 4B, 4C, and 4F). In
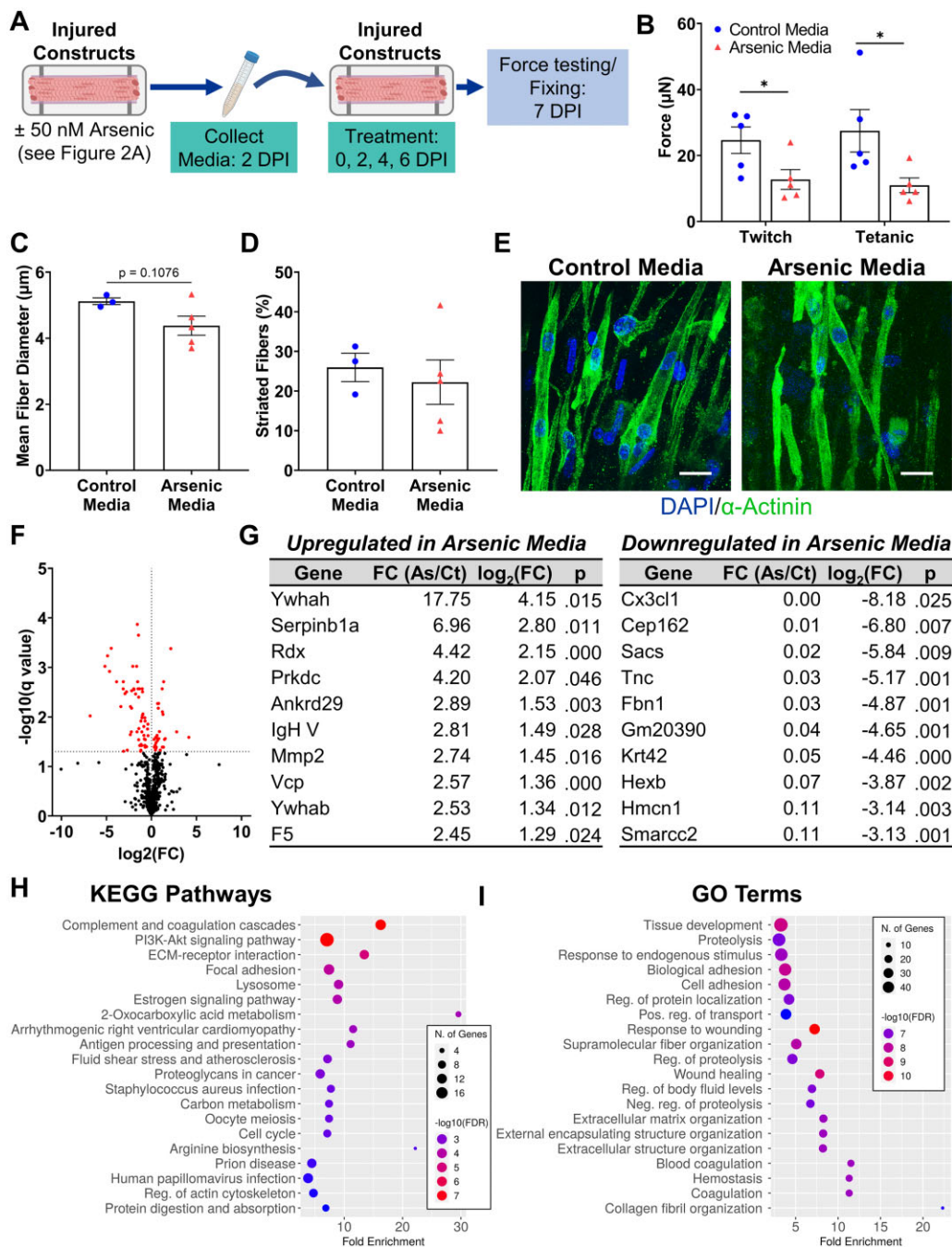
**Figure 3.** Arsenic disrupts paracrine signaling in muscle constructs. A, Experimental design for arsenic-conditioned media collection and treatment. B, Single-twitch ($N = 10$) and tetanic ($N = 10$) contractile force in conditioned-media treated muscle constructs at 7 DPI (Student's t-tests, * $p < .05$). C, Mean fiber width at 7 DPI ($N = 8$, Student's t-test). D, Percent of fibers with visible striations at 7 DPI (Student's t-test, $N = 8$). E, Representative images of constructs stained for DAPI (blue) and alpha-actinin (green, magnification = 60×, scale bar = 20 μm). F, Volcano plot of proteins identified by mass spectrometry. Differentially expressed protein cutoffs at |log2(FC)| > 0 and -log10(q) > 1.30 ($p < .05$). G, Top 10 upregulated and downregulated proteins identified via mass spectrometry in arsenic-conditioned media compared with control, sorted by fold change arsenic versus control. H, KEGG pathways and (I) GO terms identified using ShinyGO tools from differentially expressed proteins in arsenic-conditioned media.

addition, the myotube fusion index (quantified as the proportion of nuclei within eMHC+ fibers) was decreased in the As-EV or no EV treatment groups by 30% relative to Ct-EV cultures (Figs. 4D and 4F). Desmin-positive myotubes were also more than 15% smaller in the As-EV and no EV groups (Figs. 4E and 4F).

We also evaluated whether EVs from unexposed constructs could reverse the effects of arsenic exposure on myogenic differentiation. To this end, we repeated the previous experiment using C2C12 myoblasts exposed to 4 days of 50 nM arsenic prior to differentiation in low-serum (2% EV-free horse serum) media, again supplemented with Ct-EVs, As-EVs, or no EVs. Treatment of arsenic-exposed C2C12 cells with Ct-EVs resulted in 73% more eMHC positive fibers compared with cultures treated with As-EVs (Supplementary Data A—Figs. 4A and 4C). Ct-EVs also restored
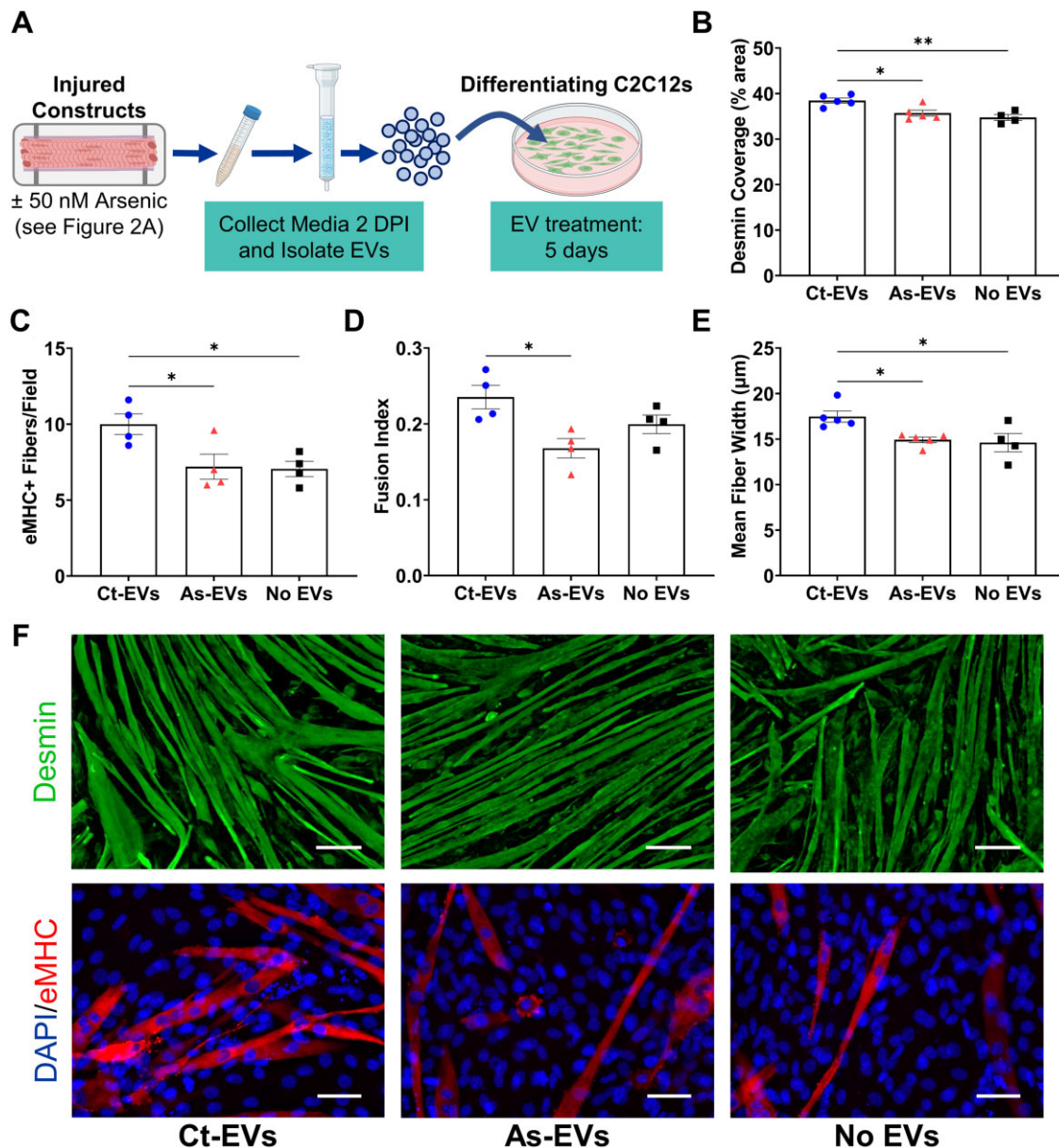
**Figure 4.** Arsenic-conditioned EVs drive impaired muscle cell differentiation. A, Experimental design for EV isolation from muscle constructs and treatment of C2C12 cells. B, Percent area showing desmin-positive signal in C2C12 cells after 5-days of EV treatment ($N = 14$, 1-way ANOVA, *$p < .05$, **$p < .01$). C, Number of embryonic-myosin heavy chain positive fibers per image ($N = 12$, 1-way ANOVA, *$p < .01$). D, Fusion index quantified as (nuclei in fused myotubes)/(total number of nuclei) ($N = 12$, 1-way ANOVA, *$p < .05$). E, Mean fiber width of desmin-positive fibers ($N = 14$, 1-way ANOVA). F, Representative images of C2C12 cells stained for desmin (top, green), DAPI (bottom, blue), and eMHC (bottom, red). Top images: Magnification = 20×, scale bars = 100 μm. Bottom images: Magnification = 40×, scale bars = 50 μm.

the fusion index of arsenic-exposed cells to levels comparable with unexposed C2C12 cells treated with Ct-EVs (Supplementary Data A—Figs. 4B and 4C).

## Arsenic affects EV signaling during *in vivo* muscle regeneration

Having shown pathogenic As-EV signaling in the myogenic cultures, we determined whether these same effects could be observed in muscle *in vivo*. Following our previously established protocol for drinking water arsenic exposure (Zhang *et al.*, 2016a), we gave male C57BL/6J mice (6 weeks old at start of experiment) 100 ppb arsenic in their water for 5 weeks then injured the TA muscles via local cardiotoxin injection. We then investigated

whether regenerative deficits may be linked to alterations in the EV-secretome during healing. Fourteen days after the injury, we harvested EVs directly from the dissected TA muscles by mincing the muscles finely in DMEM (Figure 5A). We collected the conditioned medium after 24 h, isolated EVs by SEC, and used NTA to quantify EV size distribution and number (Supplementary Data A—Figure 5). There was no difference in diameter (mean or median) nor concentration of EVs from the TA of unexposed mice (CtTA-EVs) versus EVs from the TA of arsenic-exposed animals (AsTA-EVs, Supplementary Data A—Figure 5). Comparing the effects of CtTA-EVs and AsTA-EVs on our muscle constructs with the injury-recovery assay (Figure 5A), we found that constructs receiving AsTA-EVs after injury were 40% weaker than those receiving CtTA-EVs at 7 DPI (Figure 5B). Additionally, fiber
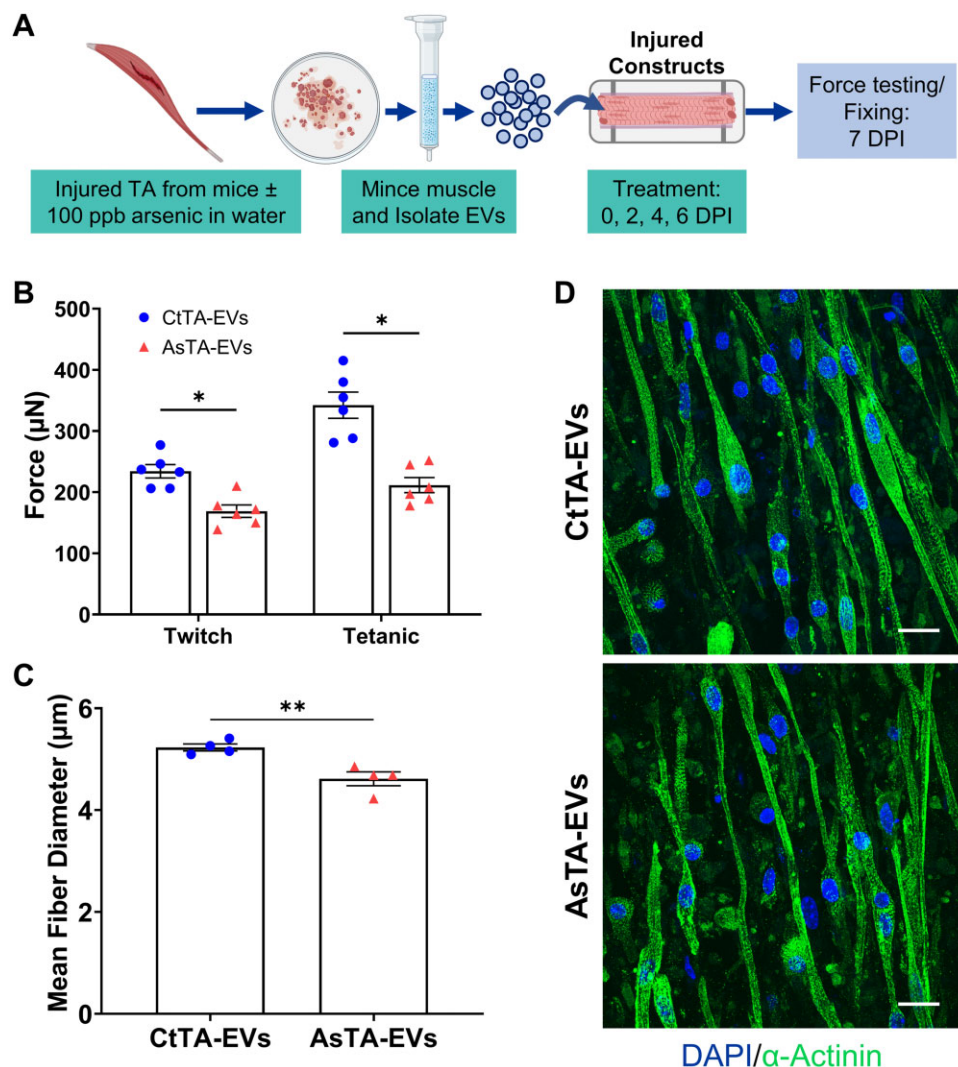
**Figure 5.** Muscles release EVs that inhibit regeneration following arsenic exposure. A, Experimental design for EV isolation from tibialis anterior muscle and treatment of muscle constructs. B, Single-twitch and tetanic contractile force in TA-EV treated muscle constructs at 7 DPI (N = 12, Student's t-tests, * p < .05). C, Mean fiber width of EV-treated constructs at 7 DPI (N = 8, Student's t-test, **p < .01). D, Representative images of constructs stained for DAPI (blue) and alpha-actinin (green, magnification = 60×, scale bar = 20 μm).

diameter in the AsTA-EVs group was 15% smaller than the CtTA-EV group (Figs. 5C and 5D). This confirmed that, during regeneration, arsenic-exposed muscles release pathogenic EVs which compromise myogenic differentiation and regeneration of mature muscle fibers.

Finally, we investigated the pathogenic As-EV effects in a fully *in vivo* model. Young C57BL/6J mice were exposed to 100 ppb arsenic in their drinking water (or normal spring water) for 5-weeks prior to a bilateral barium chloride muscle injury, which is comparable with cardiotoxin injury in its mechanism and in the regenerative response it stimulates (Hardy et al., 2016). At 1 and 3 days post injury, $7.5 \times 10^8$ of either CtTA-EVs or AsTA-EVs were injected into the injured muscles. The dose and timing was based on previous experiments showing the regenerative benefit of EVs from young mice injected into old mouse muscle following a similar paradigm (Sahu et al., 2021). After 2-weeks of recovery, we conducted *in vivo* contractile testing as previously described (Clemens et al., 2021) to quantify muscle strength, fatigability, recovery from fatigue, and physical characteristics (Figure 6A). The contractile strength data was consistent with previous observations that arsenic exposure primes muscle for poor recovery

(Anguiano et al., 2020; Zhang et al., 2016a). Animals exposed to arsenic water had approximately 20% weaker single-twitch contraction, as well as tetanic contraction than unexposed animals. However, there was no effect of CtTA-EVs versus AsTA-EVs for arsenic-exposed or unexposed animals (Figs. 6B and 6C). Arsenic-exposed groups also showed slightly heavier muscles than the control animals receiving CtTA-EVs (Figure 6D). Though, as shown above, these larger muscles did not generate stronger contractions.

We assessed fatigability and recovery from fatigue by repeatedly stimulating the muscle and quantifying force drop, then measuring recovery after 2 5-min rest windows. Recovery from fatigue was unaffected by water or EV treatment (Figure 6D). We fit 1-stage nonlinear decay models to model fatigability, generating curves which best fit the data ($R^2 > 0.8$ for all curves, Supplementary Data A—Figure 6). Comparing these models, we observed that animals receiving AsTA-EVs and either arsenic or control water fatigued to a 20% greater extent, indicated by a lower plateau of their fatigue curves. Intriguingly, CtTA-EV treatment reversed this effect in arsenic-exposed animals (Figs. 6E and 6F and Supplementary Data A—Figure 6). Overall, we
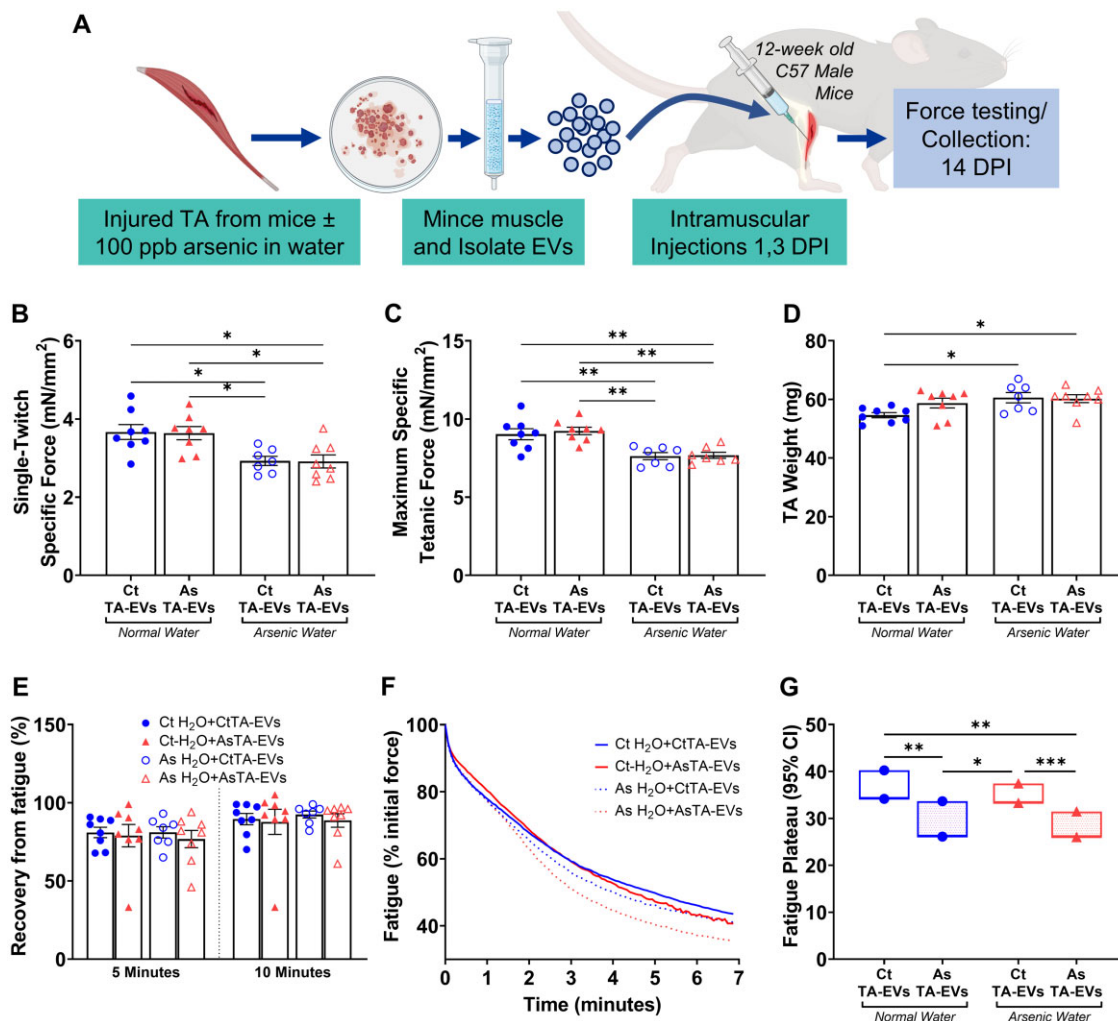
**Figure 6.** *In vivo* effects of muscle-derived EVs following arsenic exposure. A, Experimental design for EV isolation from tibialis anterior muscle and injection into regenerating muscle. B, Single-twitch force normalized to muscle cross-sectional area at 14 DPI ($N = 31$, 1-way ANOVA, *$p < .05$). C, Maximum tetanic force normalized to muscle cross-sectional area ($N = 30$, 1-way ANOVA, *$p < .05$, **$p < .01$). D, Tibialis anterior wet weight at time of dissection immediately following muscle force testing ($N = 31$, 1-way ANOVA). E, Recovery of contractile force after 5 ($N = 31$) and 10 ($N = 10$) minutes of recovery following a 7 min fatigue protocol. Data displayed as percent of initial force at the beginning of the fatigue protocol (1-way ANOVAs). F, Force curve during a 7-min fatigue protocol compromised of 105 stimulations at 4-s intervals. Lines indicate mean force ($n = 7$–8 animals per group) as a percentage of initial force at the beginning of the fatigue protocol. G, 95% confidence interval for the plateau value of nonlinear 1-phase decay models fit to the fatigue curves. Significance values calculated from post-hoc extra-sum-of-squares F tests ($N = 31$, *$p < .05$, **$p < .01$, ***$p < .001$).

confirmed that arsenic-exposure impairs muscle regeneration and found evidence that disrupted EV signaling contributes to reduced fatigue resistance of arsenic-exposed muscles. Additionally, healthy EVs demonstrated a potential therapeutic effect on fatigability in arsenic-exposed mice.

## Discussion

We employed a bioengineered 3D model of skeletal muscle fiber development and function to enhance the understanding of arsenic-promoted declines in muscle function and regenerative capacity. Our 3D muscle constructs recapitulated pathogenic effects of arsenic exposure previously observed in mouse models (Ambrosio et al., 2014; Anguiano et al., 2020; Zhang et al., 2016a) and enabled novel discovery of muscle-specific mechanisms underlying arsenic toxicity. The data strongly suggest that arsenic-induced changes in muscle-EV cargo disrupt paracrine signaling required for healthy muscle regeneration and metabolism. Further, release of pathogenic EVs from arsenic-exposed

muscle has important implications for the systemic impacts of arsenic-impaired muscle health and regeneration.

Our observation of the dramatic effects of EVs released by arsenic-conditioned muscle cells affirms the importance of EV signaling to healthy paracrine communication within muscle. The role of muscle cell-autonomous EV signaling during regeneration is established (Aswad et al., 2016; Bittel and Jaiswal, 2019) and EVs from injured myoblasts can promote myogenic differentiation and proliferation of myoblasts (Choi et al., 2016; Guescini et al., 2017). Pathogenic conditions such as high fat diet or aging can alter cargo in serum and muscle-generated EVs to impair muscle function and myogenic differentiation (Aswad et al., 2014, 2016; Rome et al., 2019). We found that, following exposure, disrupted paracrine signaling compromised a healthy regenerative response in the cultured constructs (Figure 3) and in C2C12 myoblasts (Figure 4). The finding that EVs derived from *in vivo* skeletal muscle and the pure muscle construct had similar effects (Figure 5) supports the translatability of our findings. Although we cannot be certain of the cells of origin for the TA-EVs that we

isolated, the contribution of circulating EVs was likely minimal because the tissue was extensively perfused with saline prior to muscle dissection. Therefore, the majority of EVs likely originated from myofibers themselves or other cell types resident in skeletal muscle, including progenitor cells. This further highlights the important contribution of myofiber-derived EVs during regeneration.

However, the *in vivo* findings with injected TA-EVs (Figure 6) suggest that paracrine signaling by myofiber-derived EVs only partially explains the mechanisms for arsenic impairment. The effect of TA-EVs on recovery of *in vivo* muscle force was minimal compared with the impact of the arsenic exposure. Although dosage and timing of EV administration may contribute, another possibility is that circulating EVs acting in regenerating muscle mask the effect of the injected TA-EVs. Parabiosis models have demonstrated the role of circulating factors in muscle maintenance and repair (Conboy et al., 2005; Gonzalez-Armenta et al., 2021). Recently, Sahu et al., showed that circulating EVs target areas of injury, playing an essential role in the regenerative response (Sahu et al., 2021). Our observation that mice drinking arsenic water exhibited reduced muscle force regardless of EV treatment could indicate that arsenic disrupts EV-signaling at both a muscle-specific and systemic level. Furthermore, arsenic caused muscle cells to change their release of many proteins, some of which may be soluble and not packaged within EVs. The circulating EV and soluble protein component may also play a significant role in impairing regeneration which our *in vivo* injection of muscle-derived EVs would not capture. To our knowledge, there are no studies characterizing arsenic effects on circulating EVs, but our data suggest that such experiments are warranted.

The 3D muscle construct model is a valuable tool which circumvents the limitations of traditional 2D culture and *in vivo* models of muscle-environmental interactions. The capacity to mimic and quantify muscle contractile force enhances biological and clinical relevance. Additionally, minimizing the potential confounding effects of nonmuscle cell and fiber tissue constituents, increases the value of our findings. However, the same benefits of the reductionist model might be viewed as limitations because arsenic has known effects on the vasculature, neural tissues, and connective tissue. The regenerative response is a complex cascade of events involving paracrine communication between various cell populations, culminating in activation of MuSCs, myogenic differentiation, and maturation of fibers (De Micheli et al., 2020). Our previous work elucidated the impacts of arsenic exposure on muscle fibroblasts and the vasculature that ultimately lead to dysfunctional tissue regeneration (Anguiano et al., 2020; Barchowsky et al., 1996). Nonetheless, our current findings demonstrate the important contribution of pathogenic changes in EV cargo in muscle regeneration, specifically in arsenic-induced muscle dysfunction that may contribute to the burden of arsenic promoted systemic diseases.

Though our data suggest that arsenic altered the composition of EVs released by muscle cells, the effect was probably not due to changes in size or quantity (Supplementary Data A—Figs. 3 and 5). This implies that functional outcomes associated with arsenic-conditioned EVs are driven by changes in their cargo. Arsenic-induced changes in EV cargo may lead to the delivery of molecules which repress regeneration such as NF-κB activators or pro-proliferative factors (Cheikhi et al., 2020; Zhang et al., 2016a). On the other hand, there may instead be a loss of the delivery of beneficial factors such as proregenerative mRNA (Sahu et al., 2021). Although our data cannot rule out either possibility, we highlight the importance of this question and suggest

further study into the specific gain- or loss-of-function effects associated with EV cargo. Given the diversity of the molecular cargo packaged in EVs, there is an abundance of potential candidates driving the change in EV function we observed. Future studies into arsenic-conditioned EV effects should take this into consideration.

Proteomic analysis identified several differentially expressed proteins released from the muscle constructs, likely packaged within EVs. Two of the top 10 differentially expressed proteins, Ywhah and Ywhab, belong to the 14-3-3 family of cytosolic signaling scaffold proteins. The 7 isoforms of this family are mainly protein chaperones and docking proteins, and can be packaged in exosomes (Aitken, 2011; Chavez-Muñoz et al., 2009). Five of the seven 14-3-3 isoforms were differentially abundant in arsenic-conditioned media compared with control, with 4 increasing and 1 decreasing. Each isoform has many unique binding partners and serves various tissue-dependent functions (Aitken, 2011). Intriguingly, recent attention has been given to the ability of 14-3-3 isoforms to affect the contractile function of muscle through mechanisms including regulation of ion channels and motor proteins (Koga and Ikebe, 2008; Smith et al., 2011; Thompson and Goldspink, 2021). In addition, 14-3-3 family members packaged in EVs enhance extracellular matrix protease expression in dermal fibroblasts, with implications for healthy wound healing (Chavez-Muñoz et al., 2009; Medina and Ghahary, 2010). EV-delivery of 14-3-3ζ activates the Wnt/β-catenin pathway, and several 14-3-3 isoforms regulate signaling of the FoxO transcription factor (Dobson et al., 2011; Dovrat et al., 2014; Ji et al., 2021). Wnt/β-catenin and FoxO are signaling pathways implicated in promoting arsenic-induced cardiometabolic disease (Anguiano et al., 2020; Padmaja Divya et al., 2015). The impact of arsenic exposure on 14-3-3 pathways is relatively unexplored, though 1 study suggested Ywhaz as a potential biomarker of arsenic-induced neurotoxicity (Zhang et al., 2016b). Our findings suggest further research into the role of EV-trafficked 14-3-3 in intercellular signaling following arsenic exposure.

Analysis of the differentially expressed proteins indicates changes in important cellular pathways and processes. The top KEGG pathway identified from our proteomic analysis of the arsenic-conditioned secretome was "complement and coagulation cascades." Our recent work using 3D muscle constructs to study aging also identified the complement pathways as a major disrupted pathway in aged muscle (Wang et al., 2023). This could suggest that arsenic induces an aged phenotype in muscle, essentially acting as a gerontogen (Sorrentino et al., 2014). To our knowledge, no reports have investigated this, although arsenic accelerates cartilage aging in rats (Chung et al., 2020). KEGG analysis also identified the "ECM-receptor interaction" pathway as significantly altered by arsenic. This was confirmed by significant changes in the GO terms "extracellular matrix organization" and "extracellular structure organization." Previous studies showed that arsenic causes aberrant muscle ECM remodeling and signaling (Anguiano et al., 2020; Zhang et al., 2016a), also consistent with an aged muscle phenotype (Stearns-Reider et al., 2017). Dysfunctional intercellular signaling may contribute to this response.

Our findings identify disrupted paracrine signaling, particularly through EVs, as a new mechanism of arsenic-induced muscle dysfunction. Conditioned media and EVs elaborated by constructs or muscles previously exposed to arsenic impaired muscle regeneration, mimicking the effects of direct arsenic exposure. However, it is important to reiterate that, in each model, the conditioned media and EVs were elaborated after

clearing arsenic from the system. As we have demonstrated both *in vivo* and *in vitro*, arsenic imparts an epigenetic memory of exposure (Ambrosio *et al.*, 2014; Anguiano *et al.*, 2020; Cheikhi *et al.*, 2020). This could account for the continued elaboration of EV cargo that lack proregenerative factors or contain inhibitory factors even after arsenic was removed. Arsenic effects on epigenetic regulation are mediated by arsenic-promoted mitochondrial dysfunction, with mitochondria perpetuating memory effects of arsenic-imposed stress (Ambrosio *et al.*, 2014; Anguiano *et al.*, 2020; Cheikhi *et al.*, 2019). Morphology of muscle construct mitochondria (Figure 2E) were consistent with what we found in muscle fibers *in vivo*, as well as in primary MPCs and myofibroblasts (Ambrosio *et al.*, 2014; Anguiano *et al.*, 2020; Cheikhi *et al.*, 2019). Prolonged mitochondrially driven epigenetic dysregulation could alter EV cargo including differential expression of proteins, nucleic acids, and lipids.

We also successfully validated a 3D model for studying functional and molecular impacts of arsenic exposure in skeletal muscle. The ability of our muscle constructs to recapitulate *in vivo* effects of arsenic exposure on muscle could serve as a template for future research involving the impact of other environmental exposures on EV composition and communication. Skeletal muscle receives relatively little attention in the study of environmental toxicology despite being fundamentally important to overall health as well as disease progression when dysfunctional. We anticipate that this new tool could increase the feasibility of such research and increase our understanding of muscle-related environmental diseases. Our findings implicating EV as mediators of the deleterious effects of arsenic on tissue function may extend beyond skeletal muscle. Muscles are crucial endocrine organs and EVs serve as signaling vehicles between muscles and the rest of the body, even crossing the blood-brain barrier. Thus, the mechanism we have identified could be an important step toward understanding the larger scope of arsenic-induced systemic diseases.

## Supplementary data

Supplementary data are available at *Toxicological Sciences* online.

## Declaration of conflicting interests

The authors declared no potential conflicts of interest with respect to the research, authorship, and/or publication of this article.

## Acknowledgments

## References

Aitken, A. (2011). Post-translational modification of 14-3-3 isoforms and regulation of cellular function. *Semin. Cell Dev. Biol.* **22**, 673–680.

Alamolhodaei, N. S., Shirani, K., and Karimi, G. (2015). Arsenic cardiotoxicity: An overview. *Environ. Toxicol. Pharmacol.* **40**, 1005–1014.

Ambrosio, F., Brown, E., Stolz, D., Ferrari, R., Goodpaster, B., Deasy, B., Distefano, G., Roperti, A., Cheikhi, A., Garciafigueroa, Y., *et al.* (2014). Arsenic induces sustained impairment of skeletal muscle and muscle progenitor cell ultrastructure and bioenergetics. *Free Radic. Biol. Med.* **74**, 64–73.

Anguiano, T., Sahu, A., Qian, B., Tang, W.-Y., Ambrosio, F., and Barchowsky, A. (2020). Arsenic directs stem cell fate by imparting notch signaling into the extracellular matrix niche. *Toxicol. Sci.* **177**, 494–505.

Aswad, H., Forterre, A., Wiklander, O. P. B., Vial, G., Danty-Berger, E., Jalabert, A., Lamazière, A., Meugnier, E., Pesenti, S., Ott, C., *et al.* (2014). Exosomes participate in the alteration of muscle homeostasis during lipid-induced insulin resistance in mice. *Diabetologia* **57**, 2155–2164.

Aswad, H., Jalabert, A., and Rome, S. (2016). Depleting extracellular vesicles from fetal bovine serum alters proliferation and differentiation of skeletal muscle cells in vitro. *BMC Biotechnol.* **16**, 32.

Bae, J., Jang, Y., Kim, H., Mahato, K., Schaecher, C., Kim, I. M., Kim, E., and Ro, S.-H. (2019). Arsenite exposure suppresses adipogenesis, mitochondrial biogenesis and thermogenesis via autophagy inhibition in brown adipose tissue. *Sci. Rep.* **9**, 14464.

Bain, L. J., Liu, J.-T., and League, R. E. (2016). Arsenic inhibits stem cell differentiation by altering the interplay between the Wnt3a and Notch signaling pathways. *Toxicol. Rep.* **3**, 405–413.

Balakumar, P., and Kaur, J. (2009). Arsenic exposure and cardiovascular disorders: An overview. *Cardiovasc. Toxicol.* **9**, 169–176.

Barchowsky, A., Dudek, E. J., Treadwell, M. D., and Wetterhahn, K. E. (1996). Arsenic induces oxidant stress and NF-kB activation in cultured aortic endothelial cells. *Free Radic. Biol. Med.* **21**, 783–790.

Bittel, D. C., and Jaiswal, J. K. (2019). Contribution of extracellular vesicles in rebuilding injured muscles. *Front. Physiol.* **10**, 828.

Chavez-Muñoz, C., Kilani, R. T., and Ghahary, A. (2009). Profile of exosomes related proteins released by differentiated and undifferentiated human keratinocytes. *J. Cell. Physiol.* **221**, 221–231.

Cheikhi, A., Anguiano, T., Lasak, J., Qian, B., Sahu, A., Mimiya, H., Cohen, C. C., Wipf, P., Ambrosio, F., and Barchowsky, A. (2020). Arsenic stimulates myoblast mitochondrial EGFR to impair myogenesis. *Toxicol. Sci.* **176**, 162–174.

Cheikhi, A., Wallace, C., St Croix, C., Cohen, C., Tang, W.-Y., Wipf, P., Benos, P. V., Ambrosio, F., and Barchowsky, A. (2019). Mitochondria are a substrate of cellular memory. *Free Radic. Biol. Med.* **130**, 528–541.

Chen, C.-M., Chung, M.-N., Chiu, C.-Y., Liu, S.-H., and Lan, K.-C. (2020). Inorganic arsenic exposure decreases muscle mass and enhances denervation-induced muscle atrophy in mice. *Molecules* **25**, 3057.

Choi, J. S., Yoon, H. I., Lee, K. S., Choi, Y. C., Yang, S. H., Kim, I.-S., and Cho, Y. W. (2016). Exosomes from differentiating human skeletal

muscle cells trigger myogenesis of stem cells and provide biochemical cues for skeletal muscle regeneration. *J. Control. Release* **222**, 107–115.

Chung, Y.-P., Chen, Y.-W., Weng, T.-I., Yang, R.-S., and Liu, S.-H. (2020). Arsenic induces human chondrocyte senescence and accelerates rat articular cartilage aging. *Arch. Toxicol.* **94**, 89–101.

Clarkson, E., Costa, C. F., and Machesky, L. M. (2004). Congenital myopathies: Diseases of the actin cytoskeleton. *J. Pathol.* **204**, 407–417.

Clemens, Z., Sivakumar, S., Pius, A., Sahu, A., Shinde, S., Mamiya, H., Luketich, N., Cui, J., Dixit, P., Hoeck, J. D., et al. (2021). The biphasic and age-dependent impact of klotho on hallmarks of aging and skeletal muscle function. *eLife* **10**, e61138.

Conboy, I. M., Conboy, M. J., Wagers, A. J., Girma, E. R., Weissman, I. L., and Rando, T. A. (2005). Rejuvenation of aged progenitor cells by exposure to a young systemic environment. *Nature* **433**, 760–764.

Conboy, M. J., Conboy, I. M., and Rando, T. A. (2013). Heterochronic parabiosis: Historical perspective and methodological considerations for studies of aging and longevity. *Aging Cell.* **12**, 525–530.

De Micheli, A. J., Laurilliard, E. J., Heinke, C. L., Ravichandran, H., Fraczek, P., Soueid-Baumgarten, S., De Vlaminck, I., Elemento, O., and Cosgrove, B. D. (2020). Single-cell analysis of the muscle stem cell hierarchy identifies heterotypic communication signals involved in skeletal muscle regeneration. *Cell Rep.* **30**, 3583–3595.e3585.

DeFronzo, R. A., and Tripathy, D. (2009). Skeletal muscle insulin resistance is the primary defect in type 2 diabetes. *Diabetes Care.* **32**, S157–S163.

Demonbreun, A. R., and McNally, E. M. (2017). Muscle cell communication in development and repair. *Curr. Opin. Pharmacol.* **34**, 7–14.

Dessauge, F., Schleder, C., Perruchot, M.-H., and Rouger, K. (2021). 3D in vitro models of skeletal muscle: Myopsphere, myobundle and bioprinted muscle construct. *Vet. Res.* **52**, 72–12.

Dobson, M., Ramakrishnan, G., Ma, S., Kaplun, L., Balan, V., Fridman, R., and Tzivion, G. (2011). Bimodal regulation of Foxo3 by AKT and 14-3-3. *Biochim. Biophys. Acta.* **1813**, 1453–1464.

Dovrat, S., Caspi, M., Zilberberg, A., Lahav, L., Firsow, A., Gur, H., and Rosin-Arbesfeld, R. (2014). 14-3-3 and β-catenin are secreted on extracellular vesicles to activate the oncogenic Wnt pathway. *Mol. Oncol.* **8**, 894–911.

Egan, B., and Zierath, J. R. (2013). Exercise metabolism and the molecular regulation of skeletal muscle adaptation. *Cell Metab.* **17**, 162–184.

Elia, D., Madhala, D., Ardon, E., Reshef, R., and Halevy, O. (2007). Sonic hedgehog promotes proliferation and differentiation of adult muscle cells: Involvement of MAPK/ERK and PI3K/Akt pathways. *Biochim. Biophys. Acta.* **1773**, 1438–1446.

Fleming, J., Capel, A., Rimington, R., Wheeler, P., Leonard, A., Bishop, N., Davies, O., and Lewis, M. (2020). Bioengineered human skeletal muscle capable of functional regeneration. *BMC Biol.* **18**, 145–116.

Frontera, W. R., and Ochala, J. (2015). Skeletal muscle: A brief review of structure and function. *Calcif. Tissue Int.* **96**, 183–195.

Garciafigueroa, D. Y., Klei, L. R., Ambrosio, F., and Barchowsky, A. (2013). Arsenic-stimulated lipolysis and adipose remodeling is mediated by g-protein-coupled receptors. *Toxicol. Sci.* **134**, 335–344.

Giles, B. H., and Mann, K. K. (2022). Arsenic as an immunotoxicant. *Toxicol. Appl. Pharmacol.* **454**, 116248.

Giudice, J., and Taylor, J. M. (2017). Muscle as a paracrine and endocrine organ. *Curr. Opin. Pharmacol.* **34**, 49–55.

Gonzalez-Armenta, J. L., Li, N., Lee, R.-L., Lu, B., and Molina, A. J. (2021). Heterochronic parabiosis: Old blood induces changes in mitochondrial structure and function of young mice. *J. Gerontol. A Biol. Sci. Med. Sci.* **76**, 434–439.

Goodpaster, B. H., Krishnaswami, S., Resnick, H., Kelley, D. E., Haggerty, C., Harris, T. B., Schwartz, A. V., Kritchevsky, S., and Newman, A. B. (2003). Association between regional adipose tissue distribution and both type 2 diabetes and impaired glucose tolerance in elderly men and women. *Diabetes Care.* **26**, 372–379.

Gorchev, H. G., and Ozolins, G. 1984. Who guidelines for drinking-water quality. WHO chronicle.

Guescini, M., Maggio, S., Ceccaroli, P., Battistelli, M., Annibalini, G., Piccoli, G., Sestili, P., and Stocchi, V. (2017). Extracellular vesicles released by oxidatively injured or intact C2C12 myotubes promote distinct responses converging toward myogenesis. *Int. J. Mol. Sci.* **18**, 2488.

Hall, M., Chen, Y., Ahsan, H., Slavkovich, V., Van Geen, A., Parvez, F., and Graziano, J. (2006). Blood arsenic as a biomarker of arsenic exposure: Results from a prospective study. *Toxicology* **225**, 225–233.

Hardy, D., Besnard, A., Latil, M., Jouvion, G., Briand, D., Thépenier, C., Pascal, Q., Guguin, A., Gayraud-Morel, B., Cavaillon, J.-M., et al. (2016). Comparative study of injury models for studying muscle regeneration in mice. *PLoS One.* **11**, e0147198.

Janssen, A., Leahy, A. A., Diallo, T. M., Smith, J. J., Kennedy, S. G., Eather, N., Mavilidi, M. F., Wagemakers, A., Babic, M. J., and Lubans, D. R. (2020). Cardiorespiratory fitness, muscular fitness and mental health in older adolescents: A multi-level cross-sectional analysis. *Prev. Med.* **132**, 105985.

Ji, L., Wang, Q., Liu, M., Zhu, C., Xiao, Y., Han, J., Fang, Y., Ye, J., Yin, J., and Wei, L. (2021). The 14-3-3 protein YWHAB inhibits glucagon-induced hepatic gluconeogenesis through interacting with the glucagon receptor and FOXO1. *FEBS Lett.* **595**, 1275–1288.

Koga, Y., and Ikebe, M. (2008). A novel regulatory mechanism of myosin light chain phosphorylation via binding of 14-3-3 to myosin phosphatase. *Mol. Biol. Cell.* **19**, 1062–1071.

Kumar, A., Ansari, B. A., Kim, J., Suri, A., Gaddam, S., Yenigalla, S., Vanjarapu, J. M., Selvaraj, S., Tamvada, D., Lee, J., et al. (2019). Axial muscle size as a strong predictor of death in subjects with and without heart failure. *J. Am. Heart Assoc.* **8**, e010554.

Lee, J., Kim, D., and Kim, C. (2017). Resistance training for glycemic control, muscular strength, and lean body mass in old type 2 diabetic patients: A meta-analysis. *Diabetes Ther.* **8**, 459–473.

Li, J., Xue, J., Ling, M., Sun, J., Xiao, T., Dai, X., Sun, Q., Cheng, C., Xia, H., Wei, Y., et al. (2021). MicroRNA-15b in extracellular vesicles from arsenite-treated macrophages promotes the progression of hepatocellular carcinomas by blocking the LATS1-mediated hippo pathway. *Cancer Lett.* **497**, 137–153.

Marques, A., Gomez-Baya, D., Peralta, M., Frasquilho, D., Santos, T., Martins, J., Ferrari, G., and Gaspar de Matos, M. (2020). The effect of muscular strength on depression symptoms in adults: A systematic review and meta-analysis. *Int. J Environ. Res. Public Health* **17**, 5674.

Medina, A., and Ghahary, A. (2010). Transdifferentiated circulating monocytes release exosomes containing 14-3-3 proteins with matrix metalloproteinase-1 stimulating effect for dermal fibroblasts. *Wound Repair Regen.* **18**, 245–253.

Metter, E. J., Talbot, L. A., Schrager, M., and Conwit, R. (2002). Skeletal muscle strength as a predictor of all-cause mortality in healthy men. *J. Gerontol. A Biol. Sci. Med. Sci.* **57**, B359–365.

Mitchell, R., Mellows, B., Sheard, J., Antonioli, M., Kretz, O., Chambers, D., Zeuner, M.-T., Tomkins, J. E., Denecke, B., Musante, L., et al. (2019). Secretome of adipose-derived

mesenchymal stem cells promotes skeletal muscle regeneration through synergistic action of extracellular vesicle cargo and soluble proteins. *Stem Cell Res. Ther.* **10**, 116–119.

Mondal, V., Hosen, Z., Hossen, F., Siddique, A. E., Tony, S. R., Islam, Z., Islam, M. S., Hossain, S., Islam, K., Sarker, M. K., *et al.* (2020). Arsenic exposure-related hyperglycemia is linked to insulin resistance with concomitant reduction of skeletal muscle mass. *Environ. Int.* **143**, 105890.

Mukherjee, S. C., Rahman, M. M., Chowdhury, U. K., Sengupta, M. K., Lodh, D., Chanda, C. R., Saha, K. C., and Chakraborti, D. (2003). Neuropathy in arsenic toxicity from groundwater arsenic contamination in West Bengal, India. *J. Environ. Sci. Health. A Tox. Hazard. Subst. Environ. Eng.* **38**, 165–183.

Ngalame, N. N., Luz, A. L., Makia, N., and Tokar, E. J. (2018). Arsenic alters exosome quantity and cargo to mediate stem cell recruitment into a cancer stem cell-like phenotype. *Toxicol. Sci.* **165**, 40–49.

Oberoi, S., Devleesschauwer, B., Gibb, H. J., and Barchowsky, A. (2019). Global burden of cancer and coronary heart disease resulting from dietary exposure to arsenic, 2015. *Environ. Res.* **171**, 185–192.

Padmaja Divya, S., Pratheeshkumar, P., Son, Y.-O., Vinod Roy, R., Andrew Hitron, J., Kim, D., Dai, J., Wang, L., Asha, P., Huang, B., *et al.* (2015). Arsenic induces insulin resistance in mouse adipocytes and myotubes via oxidative stress-regulated mitochondrial Sirt3-FOXO3a signaling pathway. *Toxicol. Sci.* **146**, 290–300.

Parvez, F., Wasserman, G. A., Factor-Litvak, P., Liu, X., Slavkovich, V., Siddique, A. B., Sultana, R., Sultana, R., Islam, T., Levy, D., *et al.* (2011). Arsenic exposure and motor function among children in Bangladesh. *Environ. Health Perspect.* **119**, 1665–1670.

Podgorski, J., and Berg, M. (2020). Global threat of arsenic in groundwater. *Science* **368**, 845–850.

Prakash, C., Chhikara, S., and Kumar, V. (2022). Mitochondrial dysfunction in arsenic-induced hepatotoxicity: Pathogenic and therapeutic implications. *Biol. Trace Elem. Res.* **200**, 261–270.

Rome, S., Forterre, A., Mizgier, M. L., and Bouzakri, K. (2019). Skeletal muscle-released extracellular vesicles: State of the art. *Front. Physiol.* **10**, 929.

Sahu, A., Clemens, Z. J., Shinde, S. N., Sivakumar, S., Pius, A., Bhatia, A., Picciolini, S., Carlomagno, C., Gualerzi, A., Bedoni, M., *et al.* (2021). Regulation of aged skeletal muscle regeneration by circulating extracellular vesicles. *Nat. Aging.* **1**, 1148–1161.

Sahu, A., Mamiya, H., Shinde, S. N., Cheikhi, A., Winter, L. L., Vo, N. V., Stolz, D., Roginskaya, V., Tang, W. Y., St Croix, C., *et al.* (2018). Age-related declines in alpha-Klotho drive progenitor cell mitochondrial dysfunction and impaired muscle regeneration. *Nat. Commun.* **9**, 4859.

Samuel, D., Rowe, P., Hood, V., and Nicol, A. (2012). The relationships between muscle strength, biomechanical functional moments and health-related quality of life in non-elite older adults. *Age Ageing.* **41**, 224–230.

Sarker, M. K., Tony, S. R., Siddique, A. E., Karim, M. R., Haque, N., Islam, Z., Islam, M. S., Khatun, M., Islam, J., and Hossain, S. (2021). Arsenic secondary methylation capacity is inversely

associated with arsenic exposure-related muscle mass reduction. *Int. J. Environ. Res. Public Health* **18**, 9730.

Smith, A. J., Daut, J., and Schwappach, B. (2011). Membrane proteins as 14-3-3 clients in functional regulation and intracellular transport. *Physiology (Bethesda)* **26**, 181–191.

Sorrentino, J. A., Sanoff, H. K., and Sharpless, N. E. (2014). Defining the toxicology of aging. *Trends Mol. Med.* **20**, 375–384.

States, J. C., Barchowsky, A., Cartwright, I. L., Reichard, J. F., Futscher, B. W., and Lantz, R. C. (2011). Arsenic toxicology: Translating between experimental models and human pathology. *Environ. Health Perspect.* **119**, 1356–1363.

States, J. C., Srivastava, S., Chen, Y., and Barchowsky, A. (2009). Arsenic and cardiovascular disease. *Toxicol. Sci.* **107**, 312–323.

Stearns-Reider, K. M., D'Amore, A., Beezhold, K., Rothrauff, B., Cavalli, L., Wagner, W. R., Vorp, D. A., Tsamis, A., Shinde, S., Zhang, C., *et al.* (2017). Aging of the skeletal muscle extracellular matrix drives a stem cell fibrogenic conversion. *Aging Cell.* **16**, 518–528.

Thompson, W. C., and Goldspink, P. H. (2022). 14-3-3 protein regulation of excitation-contraction coupling. *Pflugers Arch.* **474**, 267–279.

Van Niel, G., d'Angelo, G., and Raposo, G. (2018). Shedding light on the cell biology of extracellular vesicles. *Nat. Rev. Mol. Cell Biol.* **19**, 213–228.

von Haehling, S., Garfias Macedo, T., Valentova, M., Anker, M. S., Ebner, N., Bekfani, T., Haarmann, H., Schefold, J. C., Lainscak, M., Cleland, J. G. F., *et al.* (2020). Muscle wasting as an independent predictor of survival in patients with chronic heart failure. *J. Cachexia. Sarcopenia Muscle.* **11**, 1242–1249.

Wang, K., Smith, S. H., Iijima, H., Hettinger, Z. R., Mallepally, A., Shroff, S. G., and Ambrosio, F. (2023). Bioengineered 3D skeletal muscle model reveals complement 4b as a cell-autonomous mechanism of impaired regeneration with aging. *Adv. Mater.* **35**, 2207443.

Wang, P., Xiao, T., Li, J., Wang, D., Sun, J., Cheng, C., Ma, H., Xue, J., Li, Y., Zhang, A., *et al.* (2021). MiR-21 in EVs from pulmonary epithelial cells promotes myofibroblast differentiation via glycolysis in arsenic-induced pulmonary fibrosis. *Environ. Pollut.* **286**, 117259.

Yamashita, M., Kamiya, K., Matsunaga, A., Kitamura, T., Hamazaki, N., Nozaki, K., Ichikawa, T., Maekawa, E., Meguro, K., Yamaoka-Tojo, M., *et al.* (2021). Low skeletal muscle density combined with muscle dysfunction predicts adverse events after adult cardiovascular surgery. *Nutr. Metab. Cardiovasc. Dis.* **31**, 1782–1790.

Zhang, C., Ferrari, R., Beezhold, K., Stearns-Reider, K., D'Amore, A., Haschak, M., Stolz, D., Robbins, P. D., Barchowsky, A., and Ambrosio, F. (2016a). Arsenic promotes NF-Kb-mediated fibroblast dysfunction and matrix remodeling to impair muscle stem cell function. *Stem Cells* **34**, 732–742.

Zhang, J. H., Li, Y., Song, X. B., Ji, X. H., Sun, H. N., Wang, H., Fu, S. B., Zhao, L. J., and Sun, D. J. (2016b). Differential expression of serum proteins in rats subchronically exposed to arsenic identified by iTRAQ-based proteomic technology—14-3-3 ζ protein to serve as a potential biomarker. *Toxicol. Res.* **5**, 651–659.